SUPPLEMENTARY INFORMATION

Selective Isotope Labeling and LC-Photo-CIDNP Enable NMR Spectroscopy at Low-Nanomolar Concentration

Hanming Yang[a], Siyu Li[a], Clayton A. Mickles[a], Valeria Guzman-Luna[a], Kenji Sugisaki[b,c], Clayton M. Thompson, Hung H. Dang[a], and Silvia Cavagnero[a]*

[a] Department of Chemistry, University of Wisconsin - Madison, 1101 University Ave., Madison, Wisconsin, 53706, USA.

[b] Department of Chemistry, Graduate School of Science, Osaka Metropolitan University, 3-3-138 Sugimoto, Sumiyoshi-ku, Osaka, 558-8585, Japan.

[c] JST PRESTO, 4-1-8 Honcho, Kawaguchi, Saitama 332-0012, Japan.

Correspondence should be addressed to S.C. (Email: cavagnero@chem.wisc.edu, Phone: 608-262-5430).

Keywords: Hyperpolarization, photo-CIDNP, NMR, isotope labeling

Supplementary Results

1.1. Theoretical prediction of photo-CIDNP polarization arising from geminate recombination. This section focuses on the prediction of photo-CIDNP polarization arising from geminate recombination as a function of the g-factor and hyperfine coupling constants of the radicals of the photosensitizer dye and the molecule of interest. Importantly, the theoretical considerations below will also clarify how the predicted polarization of the molecule of interest depends on the isotope-labeling scheme. As stated in the article text, for freely-diffusing radical pairs, the population difference between two nuclear spin states in the reaction product is

$$p_1 - p_2 = p\left(\sqrt{|\omega_{TS1}|\,\tau_d} - \sqrt{|\omega_{TS2}|\,\tau_d}\right) \quad , \tag{S1}$$

where p_1, p_2 are the population of nuclear spin 1 and 2, p is a normalization factor, ω_{TS} is the triplet-singlet mixing frequency of a given nuclear spin state, and τ_d is the average time the radical-pair component remain within close distance before dissociating. The latter parameter can be estimated via relation

$$\tau_d = \frac{\left(R_D + R_M\right)^2}{D_D + D_M} \quad , \tag{S2}$$

where R_D and R_M are the van der Waals radii of the radicals of the dye and molecule of interest, respectively, and D_D and D_M are the corresponding translational diffusion coefficients.

The triplet-singlet (T_0 – S) mixing frequency ω_{TS} is defined according to the expressions below, where the subscript *0* denotes the nucleus of interest and χ is the spin configuration of the other nuclei

$$\omega_{TS,\alpha,\chi} = \frac{1}{2}\left[\Delta g \mu_B B_0 + \sum_i m_i A_i - \frac{1}{2}A_0 - \sum_j m_j A_j\right] \text{ and} \tag{S3}$$

$$\omega_{TS,\beta,\chi} = \frac{1}{2}\left[\Delta g \mu_B B_0 + \sum_i m_i A_i + \frac{1}{2}A_0 - \sum_j m_j A_j\right] , \tag{S4}$$

where $\omega_{TS,\alpha,\chi}$ and $\omega_{TS,\beta,\chi}$ are the triplet-singlet mixing frequencies for the configurations bearing nucleus 0 in either the α and β spin state, respectively. Δg is the difference of g-factor between dye and substrate radicals, μ_B is the Bohr's magneton, B_0 is the applied magnetic field, A_0 is the hyperfine coupling constant of nucleus *0*. In addition, m_i and A_i are the magnetic quantum number and hyperfine coupling constant of the i^{th} nucleus of the dye radical, respectively. Similarly, m_j and A_j are the magnetic quantum number and hyperfine coupling constant of the j^{th} nucleus of the molecule of interest excluding nucleus 0.

According to equation (S1), the population difference between the α, χ and β, χ nuclear-spin configurations is

$$p_{\alpha,\chi} - p_{\beta,\chi} = p\left(\sqrt{|\omega_{TS,\alpha,\chi}|\tau_d} - \sqrt{|\omega_{TS,\beta}|\tau_d}\right) . \tag{S5}$$

Now, in order to predict the polarization of nucleus *0* arising from geminate recombination, one needs to sum up all the possible nuclear spin configurations χ according to

$$P_0 = \sum_\chi p_{\alpha,\chi} - \sum_\chi p_{\beta,\chi} = p\sqrt{\tau_d}\left(\sum_\chi \sqrt{|\omega_{TS,\alpha,\chi}|} - \sum_\chi \sqrt{|\omega_{TS,\beta,\chi}|}\right) . \tag{S6}$$

The normalization factor *p* can be determined from the normalization condition according to

$$1 = \sum_{\chi} p_{\alpha,\chi} + \sum_{\chi} p_{\beta,\chi} = p\sqrt{\tau_d}\left(\sum_{\chi} \sqrt{\left|\omega_{\mathrm{TS},\alpha,\chi}\right|} + \sum_{\chi} \sqrt{\left|\omega_{\mathrm{TS},\beta,\chi}\right|} \right) \quad . \tag{S7}$$

The P_0 simulations presented in this work were carried out with a custom-built script in the Python programming language (Python v. 3.8, Python Software Foundation) and yielded P_0 according to equations (S6) and (S7). All calculations were run either on a MacOS laptop computer or at the UW-Madison Center for High-Throughput Computing (CHTC) (1, 2). The following parameters were employed: g-factor of substrate radical g($Trp^{\bullet+}$) = 2.0027 (3), diffusion coefficient of fluorescein dye $D_D = 4.2 \times 10^{-6}$ cm^2s^{-1} (4), diffusion coefficient of tryptophan substrate $D_M = 6.592 \times 10^{-6}$ cm^2s^{-1} (5), radius of $Fl^{\bullet-}$ R_D = 4.4 Å (6), radius of $Trp^{\bullet+}$ R_M = 4.2 Å (6). The hyperfine coupling constants of $Fl^{\bullet-}$ and $Trp^{\bullet+}$ were derived from the literature (3, 7). Additional details are provided in Supplementary Table S1. The hyperfine coupling constant of the Trp amino-group nitrogen was not included in the calculations, given that its value is not available in the literature to the best of our knowledge. We expect this omission not to introduce any appreciable changes to the calculation results, given that we ran a number of control calculations using either ^{15}N, ^{14}N or no N for the indole nitrogen of Trp-α-^{13}C. These control computations yielded variations in predicted polarization values by less than 7.8% (data not shown).

The above methodology enabled us to compute the expected P_0 value of Trp-U-^{13}C. The procedure adopted for the selectively labeled isotopologs Trp-α-^{13}C and Trp-α-^{13}C-

β,β,2,4,5,6,7-d_7 is analogous. In this case, one needs to set the hyperfine coupling constant to 0 when a ^{13}C is replaced by a ^{12}C (ignoring the presence of natural-abundance ^{13}C). In addition, it is necessary to multiply the hyperfine coupling constant by 0.1535 every time a ^{1}H is replaced by a ^{2}H. This multiplicative factor is equal to the ratio of gyromagnetic ratios of deuterium (D) and proton (^{1}H) according to $\gamma_D / \gamma_H = 0.1535$.

1.2. Additional considerations on overall LC-photo-CIDNP polarization. In a previous publication (8), we concluded that the overall polarization arising from LC-photo-CIDNP is

$$P_k^{M,SS} = \frac{T_1^M k_{et}^{eff} [{}^{T1}\mathrm{D}^{SS}][\mathrm{M}^{SS}](1+\gamma)\xi^G \Phi_G}{[\mathrm{M}]_0} \quad , \tag{S8}$$

where

$$\gamma = \frac{\xi^F (1-\Phi_G)}{\xi^G \Phi_G} \quad . \tag{S9}$$

In the above expressions, $P_k^{M,SS}$ denotes the steady-state polarization of nucleus *k* of the molecule of interest, T_1^M denotes the longitudinal relaxation time of nucleus *k*, k_{et}^{eff} is the composite rate constant for the bimolecular collisions (followed by electron transfer) of the molecule of interest M and the triplet excited-state dye ^{T1}D. In addition, $[^{T1}D^{SS}]$ and $[M^{SS}]$ denote the steady-state concentration of triplet excited-state dye and non-radical form of the molecule of interest, respectively. Further, γ denotes the ratio between polarization originating from the F-pair and geminate recombination events, and it is defined in equation (S9). Now, ξ^F and ξ^G denote the normalized probability difference to generate a

recombination product in the α and β spin states per recombination event for the F-pair and geminate pair, respectively. Finally, Φ_G denotes the total probability of geminate recombination per geminate radical pair.

The quantity P_0 defined in equation (S6) is defined as the normalized population difference of the α- and β- nuclear-spin states within a geminate radical pair. It is therefore evident that P_0 in equation (S6) is identical to ξ^G in equation (S8).

1.3. $^1H^\alpha$ T_2 measurements on Trp isotopologs. In order to quantify the impact of isotope substitution on $^1H^\alpha$ resonance linewidths, we carried out experiments to determine the T_2 relaxation time of different Trp isotopologs. We determined T_2 values for the three isotopologs analyzed in the main article and, in addition, unlabeled Trp, which carries all natural-abundance atoms. The pulse sequence employed for this purpose is shown in Figure S1. Briefly, this sequence features solvent pre-saturation during the recycle delay, a perfect-echo pulse scheme (9) to eliminate contributions from $J_{^1H\text{-}^1H}$ couplings, and multiple CPMG-like cycles (10, 11) to prolong the time allowed for spin-spin relaxation.

The results of the $^1H^\alpha$ T_2 measurements are shown in Figure S2. Clearly, Trp-α-^{13}C-β,β,2,4,5,6,7-d_7 has the longest T_2, nearly twice as large as that of Trp-U-^{13}C,^{15}N. This result is consistent with the qualitative observation of sharper linewidths for Trp-α-^{13}C-β,β,2,4,5,6,7-d_7. This isotopolog is expected to have longer transverse relaxation times than the other isotopologs due to the presence of the multiple deuterium substitutions.

1.4. Photo-CIDNP of Trp isotopologs at higher concentration. In addition to the LC-photo-CIDNP spectral data shown in Figure 4C of the main article, featuring 1 μM sample concentrations, similar experiments were also carried out at higher concentration (5 μM). The NMR spectra and normalized area and intensity-at-the-maximum values for the 5 μM experiments are shown in Figure S3. The results of these experiments are qualitatively consistent with those of the experiments at 1 μM concentration (Fig. 4C, main article).

1.5 Quantitative assessment of light and dark effects. The effects responsible for the observed LC-photo-CIDNP sensitivity enhancements under light (LED-on) and dark (LED-off) conditions are schematically illustrated in panel A of Supplementary Figure S4. In addition, a block diagram describing the specific experiments and computations that were performed to assess the respective quantitative contributions of LED-on and LED-off effects is provided in panel B of Supplementary Figure S4. These experiments and calculations were carried out to generate all the results shown in Table 1.

Experimental Section

Materials. The Trp-α-^{13}C-β,β,2,4,5,6,7-d$_7$ isotopolog was synthesized starting from formaldehyde-$^2H_2$ (Cambridge Isotope Laboratories, Inc.), glycine(2-^{13}C) (Cambridge Isotope Laboratories, Inc.), indole-$^2H_7$ (CDN Isotopes) and pyridoxal 5'-monophosphate (MilliporeSigma). The Trp-α-^{13}C isotopolog was prepared starting from formaldehyde

(MilliporeSigma), glycine(2-^{13}C) (Cambridge Isotope Laboratories, Inc.), indole (MilliporeSigma) and pyridoxal 5'-monophosphate (MilliporeSigma). Both isotopologs were synthesized in the presence of catalytic amounts of the *Pf* TrpB^{2B9} and *Tm* LTA enzymes (see sections below). Natural-abundance Trp was purchased from Advanced ChemTech, and uniformly labeled Trp (Trp-U-^{13}C,^{15}N) was purchased from Cambridge Isotopes Laboratories, Inc. The fluorescein photosensitizer was purchased as sodium salt (MilliporeSigma). The oxygen-scavenging enzymes *Aspergillus niger* glucose oxidase (GO, Enzyme commission classification code EC 1.1.3.4) and bovine liver catalase (CAT, EC 1.11.1.6) were purchased from MilliporeSigma as freeze-dried powders.

Preparation of *Pf* TrpB^{2B9} and *Tm* LTA Enzymes. *Pyrococcus furiosus* tryptophan synthase β-subunit 2B9 variant (*Pf* TrpB^{2B9}) (12) and *Thermotoga maritima* L-threonine aldolase (*Tm* LTA, EC 4.1.2.5) were prepared as described (13).

Preparation of GO and CAT enzyme stock solutions. GO and CAT enzyme stock solutions were prepared upon dissolving the respective enzyme powder in 10 mM potassium phosphate buffer at pH 7.2. Stock-solution concentrations were determined by electronic absorption spectroscopy using extinction coefficients 267,200 $M^{-1}cm^{-1}$ at 280 nm for GO and 912,500 $M^{-1}cm^{-1}$ at 276 nm for CAT (14). Enzyme stock solutions were aliquoted, flash-frozen with liquid nitrogen, and stored at -80 °C. Prior to LC-photo-CIDNP experiments, individual aliquots were thawed at room temperature upon incubation in a water bath.

Synthesis of Trp Isotopologs. Synthesis of Trp-α-^{13}C-β,β,2,4,5,6,7-d_7 (IUPAC name: (*S*)-2-Amino-3-[(2,4,5,6,7-$^{2}H_5$)-3-indolyl](2-^{13}C,3,3-$^{2}H_2$)propionic acid) was carried out in the presence of the *Pf* TrpB^{2B9} and *Tm* LTA enzymes according to a known enzyme-cascade procedure (13), except that we started from glycine(2-^{13}C), formaldehyde-$^{2}H_2$ and indole-$^{2}H_7$ in H_2O All stock solutions were prepared in 50 mM potassium phosphate in H_2O at pH = 8.0. The reaction was performed in 50 mM potassium phosphate in H_2O at pH = 8.0. Following heat-quenching at 90^{o}C for 15 min and centrifugation at 20,000 g for 5 min, the solution was passed through a 0.2 μm filter. Trp-α-^{13}C-β,β,2,4,5,6,7-d_7 was then purified by HPLC with a Shimadzu system comprising two LC-6AD binary pumps as well as Prominence SPD-20A ultraviolet detector and CBM-20A controller. A BioBasic 18 reverse-phase HPLC column (4.6 × 250 mm, ThermoFisher Scientific) was employed and samples were purified with a water/methanol solvent system via a gradient including a linear increase in methanol, starting from 5 to 15% (v/v) over 20 min at a 1 ml/min flow rate. HPLC purification was followed by lyophilization. Product identity and reaction yield were determined by ^{1}H-NMR. Identity was also confirmed by ESI-MS.

The second isotopolog, Trp-α-^{13}C (IUPAC name: (*S*)-2-Amino-3-(3-indolyl)(2-^{13}C)propionic acid), was synthesized, purified and characterized as above except that glycine(2-^{13}C) and natural-abundance formaldehyde and indole were employed as starting materials. Reaction yield and identity of the final product were determined by ^{1}H-NMR, with

^{13}C decoupling during acquisition using the bi_p5m4sp_4sp.2 composite pulse decoupling sequence (15). Identity was also confirmed by ESI-MS.

Preparation of Trp stock solutions. Stock solutions of natural-abundance Trp and Trp-U-^{13}C,^{15}N were prepared by dissolving the respective solid powders in distilled deionized water. Stock-solution concentrations were determined by electronic absorption spectroscopy (ext. coeff. 5,579 M^{-1} cm^{-1} at 278 nm (14)). Stock solutions of Trp-α-^{13}C and Trp-α-^{13}C-β,β,2,4,5,6,7-d_7 were also prepared by dissolving the lyophilized powders in distilled deionized water. The stock-solution concentration of these two isotopologs was assessed by ^{1}H NMR, as described below.

DFT calculations. The pK_a values and the g-factors of fluorescein radicals were calculated by density functional theory (DFT). Specifically, pK_a values were computed upon treatment of pK_a and proton energies via the AKB benchmark scheme by Matsui and coworkers (16, 17). According to the AKB procedure, the pK_a corresponding to the deprotonation reaction HA $A^- + H^+$ is determined via

$$pK_a = \frac{s\Delta G^\circ(solv)}{RT\ln 10} = \frac{s\left\{G^\circ\left(A^-\right) - G^\circ\left(HA\right)\right\}}{RT\ln 10} + \frac{sG^\circ\left(H^+\right)}{RT\ln 10} \quad . \qquad \text{(S10)}$$

Here, $G^\circ(A^-)$, G°(HA), and $G^\circ(H^+)$ are the Gibbs free energies of A^-, HA, and H^+, respectively. R denotes the universal gas constant and T is the absolute temperature; s is a scaling factor that depends on the adopted computational method. Equation (S10) can be recast as (S11) and (S12), where ΔG° is the Gibbs free energy difference $G^0(A^-) - G^0$(HA)

$$pK_a = k\Delta G° + C_0 \quad , \tag{S11}$$

$$k = \frac{s}{RT\ln 10}, C_0 = \frac{sG°\left(H^+\right)}{RT\ln 10} \quad . \tag{S12}$$

According to the AKB scheme, the scaling factor *s* and the Gibbs free energy of H^+ are optimized upon fitting experimental pK_a values of known reference molecules. In this study, we used k = 0.05219 mol kJ^{-1} and C_0 = −53.3877 kJ mol^{-1} for phenol groups, and k = 0.06448 mol kJ^{-1} and C_0 = −71.0849 kJ mol^{-1} for COOH groups (17). Geometry optimizations and Gibbs free energy calculations of fluorescein radicals were performed at the UB3LYP/6-31+G(d) level of theory. The g-factor calculations were carried out at the UB3LYP/EPR-II level in conjunction with the gauge-independent atomic orbital (GIAO) method (18, 19). In all calculations, water solvation effects were taken into account via the integral equation formalism polarizable continuum model (IEFPCM) (20). Atomic radii from the universal force field (UFF) (21) were employed to build the cavity for the IEFPCM computations. At the optimized geometries, no imaginary frequency was obtained in the vibrational mode analysis. Cartesian coordinates, energies and free energies of the fluorescein radicals are provided in Supplementary Table S2. All DFT calculations were carried out with the Gaussian 09 software (22). Overall pK_a values and g-factors at room temperature were assessed upon taking the Boltzmann distribution at 298.15 K into account.

NMR experiments under dark (LED-off) conditions. NMR samples were prepared upon diluting appropriate stock solutions in aqueous buffer (10 mM potassium phosphate adjusted

to pH 7.2). D_2O was then added to a total 10% v/v. NMR data were collected on an Avance III HD NMR spectrometer (Bruker Biospin Corp.) equipped with a 5 mm $^{1}H\{^{19}F/^{13}C/^{15}N\}$ 600 MHz triple-resonance cryogenic probe fitted with a z-gradient. Pertinent pulse sequences are as listed in the Figure legends. Unless otherwise stated, a long recycle delay (5 s) was used to ensure nearly complete spin-lattice relaxation between scans. The acquisition time was set to 2 s and 23,922 complex points. Spectra were processed with the MNova software (version 14.1.1), with zero-filling to 131,072 complex points. An exponential-decay window function was employed (0.5 Hz line-broadening). $^{1}H^{\alpha}$ resonance areas were evaluated via integration. The concentration of Trp-α-^{13}C and Trp-α-^{13}C-$\beta,\beta,2,4,5,6,7$-d_7 samples was determined upon comparing the respective $^{1}H^{\alpha}$ resonance areas to those of a natural-abundance Trp sample of known concentration in experiments employing identical acquisition and processing parameters.

The high-concentration dark ^{13}C RASPRINT experiments of Figures 4A and 4B were performed on all the above Trp samples except for natural-abundance Trp. Again, a long recycle delay (5 s) was employed to ensure nearly complete spin-lattice relaxation between scans. The acquisition time was set to 0.2048 s and 2,048 complex points were used. Spectra were processed with MNova (version 14.1.1) upon zero-filling to 65,536 complex points and 5 Hz exponential decay as window function. Area and intensity-at-the-maximum were determined with MNova. When relevant, data acquired with identical acquisition and

processing parameters were normalized upon dividing areas or intensities by sample concentration, to assess concentration-independent relative enhancements.

LC-photo-CIDNP NMR experiments under light (LED-on) conditions. LC-photo-CIDNP experiments were carried out as described (23) with the same NMR spectrometer, console and probe employed for the NMR experiments under dark conditions. A 1.5 mm-diameter and 3.5 m long polymer optical fiber (POF, Prizmatix, Holon, Israel) was used, with emission centered at 266 nm and 2.3W power at the source (UHP-mic-LED-450). The power at the fiber tip, to be inserted in a glass coaxial insert in contact with the NMR sample inside the sample tube, was 0.55 W. The ^{13}C RASPRINT pulse sequence was employed (23). Data on all isotopologs were collected with a 0.2048 s acquisition time and a 0.2 s irradiation time per scan. Experiments involving the use of the reductive radical quencher ascorbic acid (vitamin C, VC) were carried out with freshly prepared (on the same day) VC stock solutions. The final VC concentration of the NMR samples was 2 μM. This value was optimized as described (24). VC stock-solution concentrations were determined by electronic-absorption spectroscopy using the in-house measured extinction coefficient of 6,956 $M^{-1}cm^{-1}$ at 250 nm (isosbestic point, pH-independent).

LC-photo-CIDNP experiments on bacterial cell extracts. The S30 *E. coli* cell extract was prepared according to known procedures (25), as schematically illustrated in Figure 7B. LC-photo-CIDNP experiments were carried out upon mixing 140 μl of S30 extract with an

aqueous solution of Trp-α-^{13}C-β,β,2,4,5,6,7-d_7, 70 μL of D_2O and other LC-photo-CIDNP-required components (see below) up to a 700 μL final volume. The final sample contained 10 mM pH 7.2 potassium phosphate, 10% v/v D_2O, 0.15 μM glucose oxidase (GO), 0.1 μM catalase (CAT), 2.5 μM fluorescein, 1 μM Trp-α-^{13}C-β,β,2,4,5,6,7-d_7, 2.5 mM D-glucose and 5-fold diluted *E. coli* S30 cell extract.

Supplementary References

1. R. Pordes *et al.* (2007) The open science grid. in *3rd Annual Scientific Discovery through Advanced Computing Conference (SciDAC 2007)* (Boston, MA).
2. I. Sfiligoi *et al.*, The Pilot Way to Grid Resources Using glideinWMS. *WRI World Congress on Computer Science and Information Engineering* **2**, 428-432 (2009).
3. A. S. Kiryutin, O. B. Morozova, L. T. Kuhn, A. V. Yurkovskaya, P. J. Hore, ^{1}H and ^{13}C Hyperfine coupling constants of the tryptophanyl cation radical in aqueous solution from microsecond time-resolved CIDNP. *J. Phys. Chem. B* **111**, 11221-11227 (2007).
4. T. Casalini, M. Salvalaglio, G. Perale, M. Masi, C. Cavallotti, Diffusion and Aggregation of Sodium Fluorescein in Aqueous Solutions. *J. Phys. Chem. B* **115**, 12896-12904 (2011).
5. L. G. Longsworth, Diffusion Measurements, at 25°, of Aqueous Solutions of Amino Acids, Peptides and Sugars. *J. Am. Chem. Soc.* **75**, 5705-5709 (1953).
6. D. M. Togashi, B. Szczupak, A. G. Ryder, A. Calvet, M. O'Loughlin, Investigating Tryptophan Quenching of Fluorescein Fluorescence under Protolytic Equilibrium. *J. Phys. Chem. A* **113**, 2757-2767 (2009).
7. N. Shigeya, S. Yoshiharu, K. Shiro, K. Hiroshi, ESR study on fluorescein semiquinone radical. *Bull. Chem. Soc. Jpn.* **47**, 2121-2125 (1974).
8. Y. Okuno *et al.*, Laser- and cryogenic probe-assisted NMR enables hypersensitive analysis of biomolecules at submicromolar concentration. *Proc. Natl. Acad. Sci. USA* **116**, 11602-11611 (2019).
9. J. A. Aguilar, M. Nilsson, G. Bodenhausen, G. A. Morris, Spin echo NMR spectra without J modulation. *Chem. Commun.* **48**, 811-813 (2012).
10. H. Y. Carr, E. M. Purcell, Effects of diffusion on free precession in nuclear magnetic resonance experiments. *Phys. Rev.* **94**, 630-638 (1954).
11. S. Meiboom, D. Gill, Modified spin-echo method for measuring nuclear relaxatn times. *Rev. Sci. Instrum.* **29**, 688-691 (1958).
12. A. R. Buller *et al.*, Directed evolution mimics allosteric activation by stepwise tuning of the conformational ensemble. *J. Am. Chem. Soc.* **140**, 7256-7266 (2018).
13. C. M. Thompson, A. D. McDonald, H. Yang, S. Cavagnero, A. R. Buller, Modular control of L-tryptophan isotopic substitution via an efficient biosynthetic cascade. *Org. Biomol. Chem.* **18**, 4189-4192 (2020).
14. G. D. Fasman, "Handbook of biochemistry and molecular biology". (CRC Press, Cleveland (OH), 1976), vol. 1, chap. 183-203.

15. R. D. Boyer, R. Johnson, K. Krishnamurthy, Compensation of refocusing inefficiency with synchronized inversion sweep (CRISIS) in multiplicity-edited HSQC. *J. Magn. Reson.* **165**, 253-259 (2003).
16. T. Matsui, A. Oshiyama, Y. Shigeta, A Simple scheme for estimating the pK_a values of 5-substituted uracils. *Chem. Phys. Lett.* **502**, 248-252 (2011).
17. T. Matsui, Y. Shigeta, K. Morihashi, Assessment of methodology and chemical group dependences in the calculation of the pK_a for several chemical groups. *J. Chem Theory Comput.* **13**, 4791-4803 (2017).
18. R. Ditchfield, Self-consistent perturbation theory of diamagnetism. *Mol. Phys.* **27**, 789-807 (1974).
19. G. Schreckenbach, T. Ziegler, Calculation of the G-tensor of electron paramagnetic resonance spectroscopy using gauge-including atomic orbitals and density functional theory. *J. Phys. Chem. A* **101**, 3388-3399 (1997).
20. J. Tomasi, B. Mennucci, R. Cammi, Quantum mechanical continuum solvation models. *Chem. Rev.* **105**, 2999-3094 (2005).
21. A. K. Rappe, C. J. Casewit, K. S. Colwell, W. A. Goddard, W. M. Skiff, UFF, a full periodic table force field for molecular mechanics and molecular dynamics simulations. *J. Am. Chem. Soc.* **114**, 10024-10035 (1992).
22. M. Frisch *et al.*, Gaussian 09, Revision D. 01, Gaussian. *Inc., Wallingford CT* (2009).
23. H. Yang, H. Hofstetter, S. Cavagnero, Fast-pulsing LED-enhanced NMR: A convenient and inexpensive approach to increase NMR sensitivity. *J. Chem. Phys.* **151**, 245102 (2019).
24. H. Yang, M. F. Mecha, C. P. Goebel, S. Cavagnero, Enhanced nuclear-spin hyperpolarization of amino acids and proteins via reductive radical quenchers. *J. Magn. Reson.* **324**, 106912 (2021).
25. C. K. Bakke, L. M. Jungbauer, S. Cavagnero, *In vitro* expression and characterization of native apomyoglobin under low molecular crowding conditions. *Prot. Eng. Expr. Purif.* **45**, 381-392 (2006).
26. H. D. Connor, B. E. Sturgeon, C. Mottley, H. J. J. Sipe, R. P. Mason, L--Tryptophan Radical Cation Electron Spin Resonance Studies: Connecting Solution-Derived Hyperfine Coupling Constants with Protein Spectral Interpretations. *J. Am. Chem. Soc.* **130**, 6381-6387 (2008).

4. Supplementary Tables

Supplementary Table S1. Hyperfine coupling constants used for computing triplet-singlet mixing frequencies.

Specific hyperfine coupling constant	Value (mT)	Ref.	Specific hyperfine coupling constant	Value (mT)	Ref.
A ($Trp^{\bullet+}$ $^{13}C^{\alpha}$)	0.5643	(3) [a]	A ($Trp^{\bullet+}$ $^{13}C^{\eta 2}$)	0.443	(3)
A ($Trp^{\bullet+}$ $^{13}C^{\beta}$)	-0.512	(3)	A ($Trp^{\bullet+}$ $^{1}H^{\alpha}$)	0	(3)
A ($Trp^{\bullet+}$ $^{13}C'$)	-0.045	(3)	A ($Trp^{\bullet+}$ $^{1}H^{\beta 1}$)	2.544	(3)
A ($Trp^{\bullet+}$ $^{13}C^{\delta 1}$)	-0.227	(3)	A ($Trp^{\bullet+}$ $^{1}H^{\beta 2}$)	1.189	(3)
A ($Trp^{\bullet+}$ $^{13}C^{\gamma}$)	1.254	(3)	A ($Trp^{\bullet+}$ $^{1}H^{\delta 1}$)	-0.421	(3)
A ($Trp^{\bullet+}$ $^{13}C^{\delta 2}$)	-0.891	(3)	A ($Trp^{\bullet+}$ $^{1}H^{\varepsilon 1}$)	-0.413	(3)
A ($Trp^{\bullet+}$ $^{13}C^{\varepsilon 2}$)	0.092	(3)	A ($Trp^{\bullet+}$ $^{1}H^{\varepsilon 3}$)	-0.504	(3)
A ($Trp^{\bullet+}$ $^{13}C^{\varepsilon 3}$)	0.619	(3)	A ($Trp^{\bullet+}$ $^{1}H^{\zeta 2}$)	-0.050	(3)
A ($Trp^{\bullet+}$ $^{13}C^{\zeta 2}$)	-0.182	(3)	A ($Trp^{\bullet+}$ $^{1}H^{\zeta 3}$)	0.124	(3)
A ($Trp^{\bullet+}$ $^{13}C^{\zeta 3}$)	-0.499	(3)	A ($Trp^{\bullet+}$ $^{1}H^{\eta 2}$)	-0.412	(3)
A ($Fl^{\bullet-}$ ^{1}H 1,8)	0.3287	(7)	A ($Fl^{\bullet-}$ ^{1}H 14)	0.0190	(7)
A ($Fl^{\bullet-}$ ^{1}H 2,7)	0.1510	(7)	A ($Fl^{\bullet-}$ ^{1}H 15)	0.0170	(7)
A ($Fl^{\bullet-}$ ^{1}H 4,5)	0.0889	(7)	A ($Fl^{\bullet-}$ ^{1}H 16)	0.0090	(7)
A ($Fl^{\bullet-}$ ^{1}H 13)	0.022	(7)	A ($Trp^{\bullet+}$ $^{14}N^{\varepsilon 1}$)	0.20	(26)
			A ($Trp^{\bullet+}$ $^{15}N^{\varepsilon 1}$)	0.28	(26)

[a] Scaled according to the relative hyperfine coupling constant of $^{13}C^{\alpha}$ and $^{13}C^{\gamma}$ reported in the reference and DFT-simulated hyperfine coupling constant of $^{13}C^{\gamma}$ in aqueous medium.

Supplementary Table S2. Cartesian coordinates, total energies (E), Gibbs free energies (G) and g-factors (g_{iso}) for fluorescein radicals employed in the DFT calculations. All calculations were carried out assuming 1 atm and 298.15 K, therefore G values are equivalent to G^0.

$Fl^{\cdot}$ (neutral radical)

O	-1.100495	-0.561994	2.328877
O	-3.249971	-1.215315	2.387301
O	-1.116715	5.319985	-0.308815
O	5.456917	-1.344209	0.359217
O	1.958609	1.779772	0.027386
C	4.112832	-1.137234	0.192440
C	3.194061	-2.186023	0.042194
C	1.842805	-1.901819	-0.126025
C	1.349562	-0.573205	-0.158120
C	2.317609	0.452046	0.012891
C	3.670267	0.190511	0.180965
C	-0.030974	-0.218594	-0.317952
C	-0.376923	1.174501	-0.320551
C	0.643594	2.145571	-0.143630
C	-1.686378	1.681018	-0.512608
C	-1.961141	3.044726	-0.511081
C	-0.919413	3.964106	-0.320982
C	0.391880	3.510687	-0.138799
C	-1.062126	-1.264547	-0.558974
C	-1.083150	-1.892397	-1.816081
C	-2.046098	-2.848537	-2.143823
C	-3.028861	-3.196173	-1.213153
C	-3.031878	-2.586743	0.039563
C	-2.054137	-1.635287	0.384046
C	-2.052322	-1.077499	1.765897
H	3.534651	-3.218519	0.060776
H	1.143376	-2.724202	-0.234859
H	4.372192	1.008927	0.304589
H	-2.502876	0.983451	-0.669466
H	-2.979991	3.394624	-0.659157
H	1.206320	4.214343	0.000352
H	-0.334701	-1.609579	-2.551282
H	-2.032173	-3.312644	-3.126366
H	-3.785516	-3.935584	-1.459036
H	-3.785846	-2.857802	0.769972
H	-2.056640	5.522451	-0.448615
H	5.652336	-2.295947	0.350028
H	-3.153136	-0.866080	3.294035

E(UB3LYP/6-31+G(d)) = -1146.12842651 a.u.
G(UB3LYP/6-31+G(d)) = -1145.895876 a.u.
g_{iso}(UB3LYP/EPR-II) = 2.00306

Fl^{-}(-H^a) (anion radical, H^a is deprotonated)

O	-0.890153	-1.065936	2.500523
O	-3.131900	-1.056092	2.226870
O	-1.994237	5.034456	-0.348863
O	5.597520	-0.447912	0.323807
O	1.625648	2.053342	0.010574
C	4.234654	-0.466250	0.169586
C	3.500534	-1.652780	0.034027
C	2.118844	-1.597046	-0.120873
C	1.410777	-0.369413	-0.154673
C	2.198857	0.802202	-0.000683
C	3.578076	0.769822	0.155274
C	-0.012486	-0.254161	-0.300626
C	-0.579596	1.064818	-0.314967
C	0.266989	2.194667	-0.157324
C	-1.955260	1.347804	-0.508388
C	-2.450600	2.648090	-0.523441
C	-1.575027	3.728587	-0.347891
C	-0.205982	3.499703	-0.167603
C	-0.863986	-1.459100	-0.504433
C	-0.769909	-2.141580	-1.732786
C	-1.553675	-3.263185	-2.009943
C	-2.470708	-3.714407	-1.055590
C	-2.590822	-3.034672	0.157753
C	-1.791321	-1.919861	0.459885
C	-1.946930	-1.281486	1.842508
H	4.007272	-2.614615	0.053668
H	1.562430	-2.523391	-0.216689
H	4.135604	1.694202	0.267877
H	-2.643247	0.521154	-0.650356
H	-3.513138	2.824019	-0.673392
H	0.481845	4.329720	-0.041178
H	-0.071838	-1.776355	-2.482745
H	-1.453988	-3.773064	-2.964975
H	-3.090718	-4.584804	-1.256495
H	-3.312650	-3.370041	0.897642
H	5.945025	-1.355339	0.323588
H	-2.956197	5.075136	-0.479116

E(UB3LYP/6-31+G(d)) = -1145.67122707 a.u.
G(UB3LYP/6-31+G(d)) = -1145.450992 a.u.
g_{iso}(UB3LYP/EPR-II) = 2.00307

$Fl^{\bullet-}$(-H^b) (anion radical, H^b is deprotonated)

O	-1.260899	-0.485937	2.364001
O	-3.466975	-0.843494	2.125359
O	-1.378461	5.238389	-0.449632
O	5.540935	-1.095948	0.442016
O	1.904253	1.855609	-0.011791
C	4.184628	-0.956201	0.259138
C	3.315169	-2.047446	0.144880
C	1.951397	-1.828254	-0.042183
C	1.395608	-0.526877	-0.134261
C	2.317109	0.546157	0.011539
C	3.680121	0.347785	0.197745
C	-0.002535	-0.234600	-0.309238
C	-0.407050	1.140876	-0.345566
C	0.564486	2.169242	-0.191856
C	-1.734467	1.604434	-0.568185
C	-2.063471	2.948305	-0.602882
C	-1.079747	3.986066	-0.422908
C	0.263755	3.517960	-0.220444
C	-0.980797	-1.331290	-0.507611
C	-0.880330	-2.122536	-1.669014
C	-1.808414	-3.119547	-1.967954
C	-2.888038	-3.351581	-1.108336
C	-3.012584	-2.588290	0.049670
C	-2.063763	-1.599209	0.371620
C	-2.182625	-0.916601	1.689847
H	3.698811	-3.063415	0.207804
H	1.292258	-2.687108	-0.114836
H	4.342654	1.201776	0.299876
H	-2.521400	0.870533	-0.722678
H	-3.094927	3.249945	-0.776233
H	1.064185	4.243373	-0.094799
H	-0.065845	-1.924798	-2.360624
H	-1.698499	-3.702402	-2.878901
H	-3.622317	-4.118858	-1.336613
H	-3.837778	-2.769547	0.730021
H	5.774689	-2.038360	0.468586
H	-3.453369	-0.440455	3.014757

E(UB3LYP/6-31+G(d)) = -1145.66006120 a.u.

G(UB3LYP/6-31+G(d)) = -1145.440251 a.u.

g_{iso}(UB3LYP/EPR-II) = 2.00343

$Fl^{\bullet-}$(-H^c) (anion radical, H^c is deprotonated)

O	-1.287650	-0.459824	2.340654
O	-3.476594	-0.915087	2.120742
O	-1.199079	5.247515	-0.439035
O	5.547114	-1.267873	0.458031
O	1.970408	1.797907	-0.003611
C	4.288546	-1.057213	0.288701
C	3.329855	-2.127340	0.173164
C	1.978946	-1.892078	-0.012261
C	1.431619	-0.580888	-0.113212
C	2.378784	0.472745	0.027757
C	3.732170	0.265934	0.213377
C	0.041361	-0.275787	-0.283571
C	-0.349270	1.110602	-0.319726
C	0.645236	2.115316	-0.175723
C	-1.667275	1.583740	-0.538328
C	-1.979216	2.941257	-0.580712
C	-0.965540	3.892112	-0.412103
C	0.354627	3.474704	-0.213157
C	-0.950501	-1.354812	-0.500902
C	-0.834126	-2.146931	-1.660966
C	-1.768715	-3.129270	-1.984121
C	-2.871019	-3.348976	-1.149314
C	-3.010027	-2.588755	0.008128
C	-2.055981	-1.611711	0.355434
C	-2.193395	-0.934467	1.673358
H	3.698117	-3.149163	0.244992
H	1.303020	-2.740365	-0.078234
H	4.392805	1.124115	0.311815
H	-2.467959	0.865967	-0.685753
H	-3.006413	3.257349	-0.748035
H	1.152476	4.201589	-0.095805
H	-0.000354	-1.959365	-2.331746
H	-1.646368	-3.710856	-2.894308
H	-3.610546	-4.105264	-1.396562
H	-3.851464	-2.762513	0.669962
H	-2.143015	5.416657	-0.593836
H	-3.470369	-0.508330	3.008338

E(UB3LYP/6-31+G(d)) = -1145.66019548 a.u.

G(UB3LYP/6-31+G(d)) = -1145.440367 a.u.

g_{iso}(UB3LYP/EPR-II) = 2.00346

$Fl^{\cdot 2-}$(-H^a, -H^b) (dianion radical, H^a and H^b are deprotonated)

O	-1.047034	-1.075935	2.559268
O	-3.235251	-0.690743	2.158858
O	-1.644786	5.198063	-0.379719
O	5.542942	-0.866581	0.330930
O	1.779121	1.947399	0.016070
C	4.176815	-0.777725	0.175184
C	3.351331	-1.899313	0.040239
C	1.975467	-1.731456	-0.116368
C	1.364378	-0.451593	-0.152780
C	2.246194	0.654579	0.002543
C	3.618824	0.507037	0.159208
C	-0.044772	-0.216111	-0.297933
C	-0.503297	1.141964	-0.312695
C	0.425891	2.208821	-0.157652
C	-1.851993	1.549605	-0.511280
C	-2.237457	2.880346	-0.532642
C	-1.296048	3.956163	-0.361019
C	0.068372	3.543808	-0.173337
C	-0.986792	-1.352253	-0.503978
C	-0.937170	-2.047075	-1.729335
C	-1.798846	-3.108352	-2.012624
C	-2.755956	-3.488043	-1.066137
C	-2.833850	-2.797273	0.144545
C	-1.955007	-1.744261	0.451665
C	-2.082398	-1.102270	1.834451
H	3.778535	-2.899692	0.060930
H	1.347824	-2.611621	-0.211440
H	4.249099	1.383969	0.272137
H	-2.605381	0.778329	-0.647173
H	-3.283671	3.139639	-0.686733
H	0.838085	4.302126	-0.048125
H	-0.207142	-1.736989	-2.473996
H	-1.729163	-3.626025	-2.966437
H	-3.438206	-4.309850	-1.270678
H	-3.585298	-3.077611	0.878451
H	5.813275	-1.799483	0.329482

E(UB3LYP/6-31+G(d)) = -1145.20048714 a.u.
G(UB3LYP/6-31+G(d)) = -1144.993028 a.u.
g_{iso}(UB3LYP/EPR-II) = 2.00338

$Fl^{\cdot 2-}$(-H^a, -H^c) (dianion radical, H^a and H^c are deprotonated)

O	-1.033793	-1.114181	2.563555
O	-3.221202	-0.814938	2.092020
O	-1.773075	5.103450	-0.373200
O	5.617785	-0.710754	0.344939
O	1.738377	1.989269	0.017246
C	4.338158	-0.625133	0.205794
C	3.490349	-1.781989	0.080378
C	2.117421	-1.680086	-0.076732
C	1.439171	-0.430046	-0.131497
C	2.278684	0.709738	0.014954
C	3.650273	0.636660	0.171375
C	0.022697	-0.264300	-0.281903
C	-0.500563	1.073432	-0.308524
C	0.387174	2.175122	-0.155132
C	-1.862598	1.409834	-0.517600
C	-2.312011	2.729752	-0.542745
C	-1.401179	3.776918	-0.365145
C	-0.042096	3.496468	-0.175762
C	-0.868991	-1.438752	-0.491996
C	-0.755793	-2.155496	-1.700712
C	-1.568704	-3.253172	-1.988351
C	-2.540213	-3.650523	-1.063811
C	-2.681109	-2.939957	0.129490
C	-1.852001	-1.848840	0.441602
C	-2.044921	-1.189487	1.808751
H	3.961364	-2.763003	0.115210
H	1.527019	-2.588757	-0.160543
H	4.223049	1.555539	0.275427
H	-2.580969	0.609094	-0.658093
H	-3.367024	2.942024	-0.701900
H	0.675367	4.301806	-0.050552
H	-0.014556	-1.832824	-2.428439
H	-1.450559	-3.785859	-2.929033
H	-3.184903	-4.501209	-1.272088
H	-3.443561	-3.234651	0.846328
H	-2.732455	5.174227	-0.507389

E(UB3LYP/6-31+G(d)) = -1145.20065790 a.u.
G(UB3LYP/6-31+G(d)) = -1144.992835 a.u.
g_{iso}(UB3LYP/EPR-II) = 2.00340

$Fl^{\cdot 2-}$(-H^b, -H^c) (dianion radical, H^b and H^c are deprotonated)

O	-1.561907	-0.140467	2.247366
O	-3.707933	-0.771107	2.027936
O	-0.963318	5.302758	-0.525826
O	5.499348	-1.509164	0.503575
O	2.080546	1.714581	-0.043631
C	4.249751	-1.238173	0.336310
C	3.234263	-2.260133	0.282851
C	1.895961	-1.961115	0.099638
C	1.413746	-0.630853	-0.067875
C	2.413722	0.376573	0.027260
C	3.760217	0.103953	0.210107
C	0.030119	-0.262348	-0.235755
C	-0.281423	1.145223	-0.284740
C	0.762718	2.104845	-0.190706
C	-1.572778	1.699813	-0.508098
C	-1.807011	3.060168	-0.593153
C	-0.749769	4.031783	-0.462247
C	0.555316	3.474605	-0.266052
C	-0.992492	-1.295087	-0.446170
C	-0.807213	-2.201052	-1.520183
C	-1.777856	-3.117163	-1.903076
C	-3.000716	-3.179637	-1.205809
C	-3.203101	-2.340508	-0.121628
C	-2.212638	-1.417967	0.299673
C	-2.414944	-0.713863	1.575692
H	3.546823	-3.295708	0.407766
H	1.177445	-2.775892	0.093932
H	4.462945	0.932096	0.271018
H	-2.414319	1.022286	-0.623656
H	-2.817926	3.427494	-0.762921
H	1.410400	4.142335	-0.186641
H	0.109037	-2.126829	-2.099029
H	-1.601588	-3.763440	-2.759529
H	-3.774234	-3.880917	-1.506817
H	-4.129105	-2.403497	0.439192
H	-3.718598	-0.325116	2.895107

E(UB3LYP/6-31+G(d)) = -1145.18697715 a.u.
G(UB3LYP/6-31+G(d)) = -1144.979506 a.u.
g_{iso}(UB3LYP/EPR-II) = 2.00351

$Fl^{\cdot 3-}$ (trianion radical)

O	-1.227879	-0.941179	2.564402
O	-3.368602	-0.444474	2.054834
O	-1.263532	5.286997	-0.426243
O	5.516696	-1.271533	0.381723
O	1.939582	1.819201	0.016537
C	4.247314	-1.055119	0.227548
C	3.285718	-2.113832	0.097058
C	1.928074	-1.866639	-0.068916
C	1.381204	-0.555185	-0.130684
C	2.334942	0.490182	0.016912
C	3.693411	0.268131	0.182820
C	-0.014906	-0.237072	-0.277195
C	-0.390118	1.152043	-0.302346
C	0.606204	2.157654	-0.159997
C	-1.704950	1.649386	-0.516622
C	-2.003829	3.005845	-0.557012
C	-0.998137	4.017915	-0.392783
C	0.332064	3.516234	-0.195894
C	-1.020661	-1.312630	-0.485323
C	-0.954257	-2.070096	-1.674876
C	-1.873474	-3.078256	-1.969016
C	-2.914312	-3.343834	-1.072378
C	-3.008714	-2.595637	0.102475
C	-2.070569	-1.599043	0.424504
C	-2.225503	-0.921563	1.787434
H	3.647410	-3.140641	0.137681
H	1.248156	-2.711016	-0.151224
H	4.358822	1.122883	0.288377
H	-2.509896	0.931280	-0.650149
H	-3.031549	3.328216	-0.720884
H	1.151705	4.222934	-0.080296
H	-0.161485	-1.846752	-2.385529
H	-1.785356	-3.641317	-2.895546
H	-3.644824	-4.120532	-1.286879
H	-3.820109	-2.788052	0.800171

E(UB3LYP/6-31+G(d)) = -1144.72364361 a.u.
G(UB3LYP/6-31+G(d)) = -1144.529698 a.u.
g_{iso}(UB3LYP/EPR-II) = 2.00358

5. Supplementary Figure Legends

Supplementary Figure S1. NMR pulse sequence used for $^{1}H^{\alpha}$ T_2 measurements. $^{1}H^{\alpha}$ T_2 values of different Trp isotopologs were measured with a pulse sequence employing a perfect-echo CPMG-like pulse scheme (9) including solvent pre-saturation. The duration of each CPMG-like block was 50 ms, with the delay τ set to 12.5 ms. To avoid artifacts, it was important to keep the τ value fairly short. The different time points for the T_2 measurements (see Fig. S2) were obtained upon varying the number of CPMG-like iterations n.

Supplementary Figure S2. Results of $^{1}H^{\alpha}$ T_2 measurements. Data were collected with the pulse sequence in Figure S1. As part of the data processing, areas of individual $^{1}H^{\alpha}$ resonances were determined and plotted as a function of the total CPMG-like duration. The data were fit to a single exponential decay to determine the transverse relaxation time constant T_2. The resulting T_2 values of each isotopolog are annotated on the plot. Data are displayed as avg ± S.E. (n=3). A 121.5 Hz field solvent-presaturation scheme was applied during the entire 5 s recycle delay.

Supplementary Figure S3. LC-photo-CIDNP spectra of 5 μM Trp isotopologs. (a) LC-photo-CIDNP spectra of Trp isotopologs acquired with the 1D ^{13}C RASPRINT pulse sequence under both light (LED-on) and dark (LED-off) conditions. The concentration of each sample was 5 μM. (b) Analysis of normalized H^{α} areas and intensities-at-the-maximum under light (LED-on) conditions. Values were normalized relative to the uniformly labeled Trp-U-^{13}C,^{15}N isotopolog.

Supplementary Figure S4. Quantitative evaluations of light-on and light-off effects. (a) Schematic representation of the effects responsible for the observed LC-photo-CIDNP sensitivity enhancements under light (LED-on) and dark (LED-off) conditions. (b) Block diagram representing the specific experiments and computations carried out to quantitatively assess the contribution of LED-on and LED-off effects to the observed nuclear-spin hyperpolarization.

6. Supplementary Figures

Supplementary Figure S1

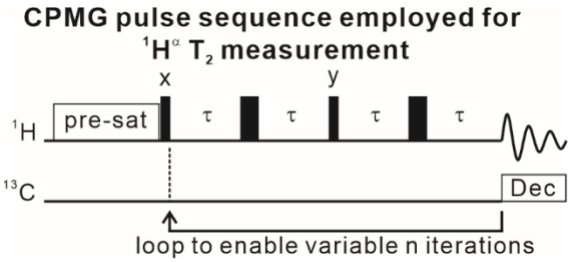

Supplementary Figure S2

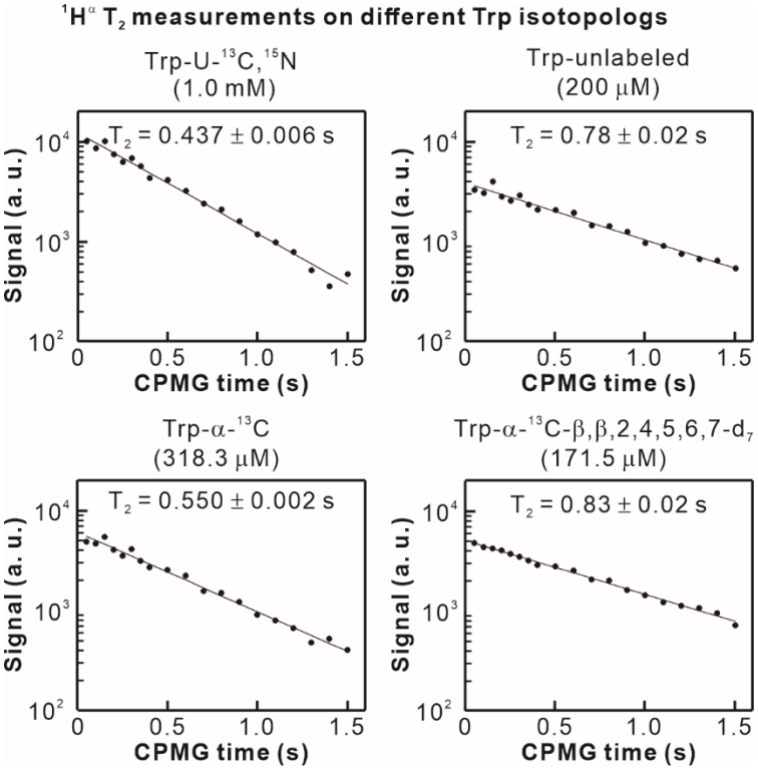

Supplementary Figure S3

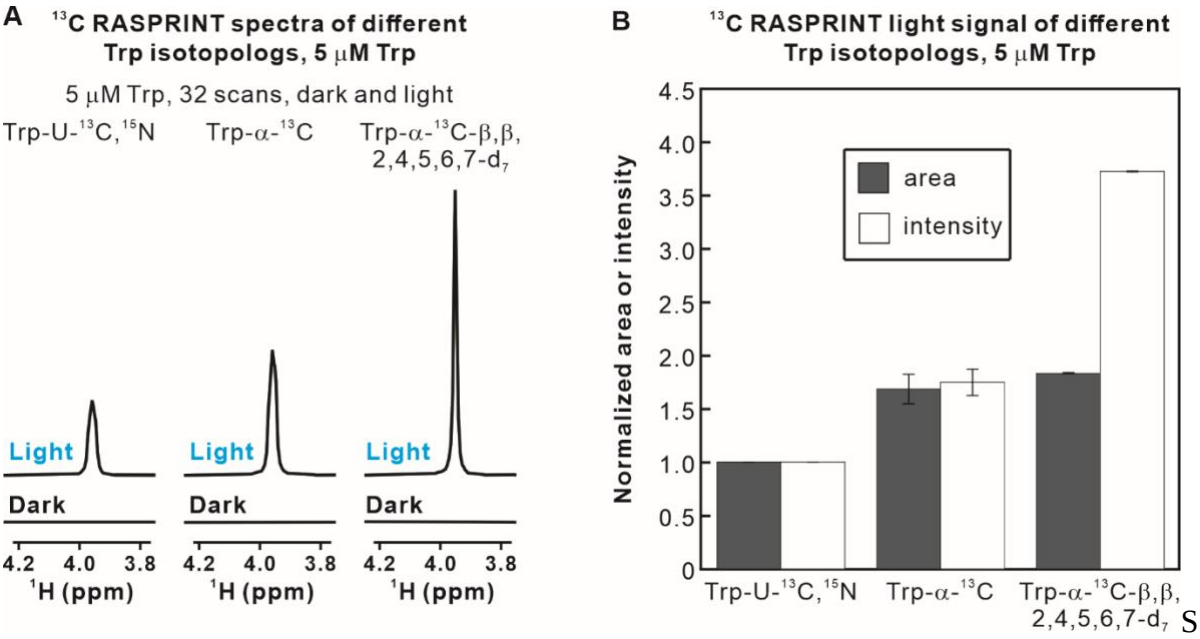

S

Supplementary Figure S4